JCI insight

KCNQ/M-channels regulate mouse vagal bronchopulmonary C-fiber excitability and cough sensitivity

Hui Sun, … , Lu-Yuan Lee, Bradley J. Undem

JCI Insight. 2019. https://doi.org/10.1172/jci.insight.124467.

Research In-Press Preview **Pulmonology**

Increased airway vagal sensory C-fiber activity contributes to the symptoms of inflammatory airway diseases. The KCNQ/K_v7/M-channel is a well-known determinant of neuronal excitability, yet whether it regulates the activity of vagal bronchopulmonary C-fibers and airway reflex sensitivity remain unknown. Here we addressed this issue using single-cell RT-PCR, patch clamp technique, extracellular recording of single vagal nerve fibers innervating the mouse lungs, and telemetric recording of cough in free-moving mice. Single-cell mRNA analysis and biophysical properties of M-current (I_M) indicate that KCNQ3/K_v7.3 is the major M-channel subunit in mouse nodose neurons. The M-channel opener retigabine negatively shifted the voltage-dependent activation of I_M, leading to membrane hyperpolarization, increased rheobase and suppression of both evoked and spontaneous action potential (AP) firing in nodose neurons in the M-channel inhibitor XE991-sensitive manner. Retigabine also markedly suppressed the α,β-methylene ATP-induced AP firing in nodose C-fiber terminals innervating the mouse lungs, and irritant gases-evoked coughing in awake mice. In conclusion, KCNQ/M-channels play a role in regulating the excitability of vagal airway C-fibers at both the cell soma and nerve terminals. Drugs that open M-channels in airway sensory afferents may relieve the sufferings associated with pulmonary inflammatory diseases such as chronic coughing.

KCNQ/M-channels Regulate Mouse Vagal Bronchopulmonary C-fiber Excitability and Cough Sensitivity

Hui Sun,[1] An-Hsuan Lin,[2] Fei Ru[1] , Mayur J. Patil,[1] Sonya Meeker,[1] Lu-Yuan Lee[2] and Bradley J. Undem[1]

1. Department of Medicine, Johns Hopkins University School of Medicine, Baltimore, Maryland;

2. Department of Physiology, University of Kentucky, Lexington, Kentucky

Corresponding author: Bradley J. Undem, 5501 Hopkins Bayview Circle, JHAAC 3A.44, Baltimore, Maryland 20224. Phone: 410 550 2160. Email: bundem@jhmi.edu

Conflict of interest: The authors have declared that no conflict of interest exists

Abstract

Increased airway vagal sensory C-fiber activity contributes to the symptoms of inflammatory airway diseases. The KCNQ/K_v7/M-channel is a well-known determinant of neuronal excitability, yet whether it regulates the activity of vagal bronchopulmonary C-fibers and airway reflex sensitivity remains unknown. Here we addressed this issue using single-cell RT-PCR, patch clamp technique, extracellular recording of single vagal nerve fibers innervating the mouse lungs, and telemetric recording of cough in free-moving mice. Single-cell mRNA analysis and biophysical properties of M-current (I_M) suggest that KCNQ3/K_v7.3 is the major M-channel subunit in mouse nodose neurons. The M-channel opener retigabine negatively shifted the voltage-dependent activation of I_M, leading to membrane hyperpolarization, increased rheobase and suppression of both evoked and spontaneous action potential (AP) firing in nodose neurons in the M-channel inhibitor XE991-sensitive manner. Retigabine also markedly suppressed the α,β-methylene ATP-induced AP firing in nodose C-fiber terminals innervating the mouse lungs, and irritant gases-evoked coughing in awake mice . In conclusion, KCNQ/M-channels play a role in regulating the excitability of vagal airway C-fibers at both the cell soma and nerve terminals. Drugs that open M-channels in airway sensory afferents may relieve the sufferings associated with pulmonary inflammatory diseases such as chronic coughing.

Introduction

K_v7 subfamily of voltage-gated potassium channels, encoded by *KCNQ* genes, exerts critical physiological functions. This is highlighted by the fact that mutations, that occur in every member of the *KCNQ* gene family, cause human genetic disorders such as long-QT syndrome with fatal cardiac arrhythmias, epilepsy, encephalopathy, myokymia, deafness and a congenital neurological disorder with intellectual disability (1, 2). Of the currently identified five members of *KCNQ* genes, *KCNQ2-5*, coding for the pore-forming $K_v7.2$-7.5 α-subunits, are expressed in the nervous system and generate a low threshold-activated and non-inactivating K^+ current, originally termed M-current (I_M) when it was first identified in the sympathetic neurons as a K^+ conductance suppressed by muscarinic receptor activation (3). The KCNQ/K_v7 channels underlying the M-current, also called M-channels, are ideally suited to control and regulate the neuronal membrane potential and excitability because they are constitutively activated at subthreshold potentials and subject to modulation by an array of neurotransmitters and inflammatory mediators signaling through the $G_{q/11}$-coupled receptors (4, 5).

Since the discovery of *KCNQ2/3* mutations associated with human early-onset epilepsies 20 years ago (6-8), the KCNQ/M-channels have been extensively studied in the brain. Compelling evidence has established the KCNQ/M-channel as a potential target for the treatment of a wide range of hyperexcitability-associated neuronal and psychiatric disorders (9, 10), and particularly, led to the approval of M-channel opener retigabine for clinical use to treat certain forms of epilepsy (11). Functional M-channels have also been found throughout the somatosensory system from afferent terminals to central neurons in spinal cord and thalamus, and increasingly are recognized as playing a role in pain signaling(12-14). Opening M-channel

attenuates nociceptive behaviors in various animal models of pain, including inflammatory, neuropathic and cancer pain(13, 15).

By contrast, whether KCNQ/M-channels contribute to the regulation of airway sensory afferent excitability has not been explored. In fact, studies of M-channels in the visceral sensory system have been sparse and limited to the modulation of aorta baroreceptor activities (16) and nociception in gut tissues (17, 18). Airway sensory afferent nerves, mainly derived from neurons in the vagal sensory ganglia, are critical in initiating reflex responses to harmful stimuli to protect the airways and fine-tune the cardiopulmonary functions. The majority of vagal sensory afferents terminating in the respiratory tract are C-fibers that are characterized by expression of TRPV1. When stimulated C-fibers mediate urge-to-cough, dyspnea, as well as parasympathetic reflex mucus secretion and bronchoconstriction. C-fibers can be activated by mediators of inflammation, contributing to negative symptoms in inflammatory airway diseases (reflex bronchospasm, secretions, and non-productive coughing) (19). Therefore, ion channels that control the excitability of airway vagal C-fibers may be an attractive therapeutic target aimed at reducing the suffering of those with inflammatory airways diseases. In this study, we address the hypotheses that M-channels play a role in regulating the excitability of vagal C-fibers in the mouse lungs, and that opening the M-channel inhibits C-fiber-mediated coughing. We characterized the expression of KCNQ genes in airway-specific mouse nodose neurons, critically evaluated I_M in nodose neurons, determined the role of M-channels in regulating the excitability of nodose neurons and C-fiber terminals innervating the lungs, and assessed the effects of M-channel opener retigabine on irritant gases-induced cough in freely moving mice.

Results

KCNQ gene expression in mouse nodose neurons and lung-specific nodose neurons

We first examined the KCNQ gene expression in mouse nodose ganglia and found that *Kcnq2-5*, but not *Kcnq1* (using mouse heart as positive control), are consistently expressed. We then further characterized the *Kcnq2-5* expression profile in the single-neuron level to gain insight into the possible subunit compositions of M-channels in mouse nodose neurons. *P2rx2* transcript was used as the marker of nodose neurons (*vs.* jugular neurons) and T*rpv1* as the marker for capsaicin-sensitive C-fibers (20). We evaluated nodose neurons in general as well as nodose neurons retrogradely labeled by dye injection into the lungs. The *Kcnq* expression patterns were not substantially different between the general population of nodose neurons and lung-specific nodose neurons. As shown in Figure 1, the expression of *Kcnq3* mRNA is most prevalent in both unlabeled (24/30 cells) and lung-specific (22/30 cells) mouse nodose neurons, and in both *Trpv1*-positive and *Trpv1*-negative groups. *Kcnq2* mRNA was detected in about half of neurons with slightly higher incidence being observed in *Trpv1*-negative groups of both unlabeled (60% vs. 40%) and lung-specific (53% vs. 31%) nodose neurons. About 10% of neurons in both labeled and unlabeled groups expressed *Kcnq5*, mostly in *Trpv1*-positive neurons. *Kcnq4* transcript was rarely detected. It is interesting to note that about 50% of *Trpv1*-positive nodose neurons expressed solely *Kcnq3,* whereas the majority of *Trpv1*-negative neurons co-expressed *Kcnq3* and *Kcnq2*. Only 1-2 *Trpv1*-negative neurons expressed *Kcnq3* alone.

Characterization of M-currents in mouse nodose neurons

Because of the very similar *Kcnq* expression profiles in unlabeled and lung-specific mouse nodose neurons, we performed patch clamp recordings in unlabeled nodose neurons. The voltage-clamp protocol shown in Fig. 2A and M-channel blocker XE991 were used to isolate I_M. Representative recordings obtained from one nodose neuron before, during bath application of XE991 and after washout of the drug are shown in Fig. 2A (upper panels). XE991 (10μM) markedly reduced the holding current at -30 mV , abolished the currents elicited by hyperpolarizing steps, partially inhibited the currents induced by depolarization to ≥-15 mV, significantly attenuated the tail currents recorded at -60 mV (I_{tail}) and completely blocked the slowly activating current elicited by stepping back to holding potential (V_h) from -60 mV. Upon washout of XE991, the inhibition of currents observed at voltages ≥-5 mV was largely relieved. However, the inhibitory effects of XE991 on currents recorded at voltages negative to -15 mV (including the currents reactivated by steps from -60 mV to V_h) and the corresponding I_{tail} could not be reversed by washout of the drug, suggesting that these currents are mediated by M-channels which have been showed to be irreversibly blocked by XE991 (21, 22). These effects are well illustrated with the total XE991-sensitive currents, obtained by digital subtraction of currents recorded in the presence of XE991 from those recorded under control conditions; the reversible XE991-sensitive current, obtained by digital subtraction of currents recorded in the presence of XE991 from those recorded after washout of the drug; and the irreversible XE991-sensitive currents, derived by digital subtraction of currents recorded after washout of XE991 from those under control condition (Fig. 2A, lower panels). The latter is smaller in amplitude and mainly a non-inactivating current component that appears to reach its maximum around -15 mV, then decreases at more positive potentials (for the sake of clarity, only current traces

recorded up to -5 mV are shown). By contrast, the currents reversibly blocked by XE991, believed to be mediated by $K_v2.1$ channels (21), activate at more positive voltages, have a different kinetics and are associated with a smaller and faster I_{tail}.

We further characterized the sustained component of *irreversible* XE991-sensitive currents. The apparent reversal potential (E_{rev}) was determined by examining the current-voltage (I-V) relationships of instantaneous (I_{in}) and sustained currents (I_{ss}) induced by hyperpolarizing steps from V_h to -85 through -35 mV during the first voltage pulse (Fig. 2B). The intersection of two I-V curves gave an estimate of E_{rev}, which was found to be -81.4±0.7 mV (n=9), closely similar to the calculated E_K (-83.2 mV) based on the K^+ concentrations in bath and pipette solutions.

The deactivation of irreversible XE991-sensitive currents elicited by hyperpolarization from V_h to -75 through -45 mV was best-fitted by a biexponential function. The mean fast (τ_{fast}) and slow time constants (τ_{slow}) obtained from 5 cells where the current was large enough for accurate curve fitting are plotted against the voltage in Fig. 2C. Both τ_{fast} and τ_{slow} have tendency to be faster at more negative voltages between -45 and -65 mV (p=0.06, two-way ANOVA). The activation of the current induced by stepping back to V_h following a full deactivation at -60 mV was best fitted to a monoexponential function with a time constant of 205±34 ms (n=9).

The voltage-dependent activation properties of XE991-sensitive currents were determined by analyzing I_{tail} whose amplitude reflects the fraction of channels opened at the end of prior voltage steps (V_m). The amplitude of total, reversible and irreversible XE991-sensitive I_{tail} obtained from the cell shown in Fig. 2A is plotted against V_m in the left panel of Fig.

2D. Both total and irreversible XE991-sensitive currents activates around -65mV and follow the same trajectory up to -25 mV. The irreversible component reaches plateau at -15 mV, 10 mV negative than the total XE991-sensitive I_{tail}. The reversible component activates around -15 mV and contributes significantly to the XE991-sensitive I_{tail} at potentials ≥ -5 mV. 8/9 neurons studied exhibited a reversible XE991-sensitive component. In 4/8 cells the irreversible XE991-sensitive I_{tail} dominated over the entire examined voltage range as the one shown in Fig. 2D (left). In the other 4 cells, the reversible, non-I_M component is much larger at positive voltages as the example given in the right panel of Fig. 2D. In both cases, however, the activation of irreversible XE991-sensitive currents declines after reaching the maximum. This inward rectification at more positive potentials was observed in 8/9 neurons. The response to capsaicin was tested in 7/9 neurons. The degree of inward rectification, measured as the percentage of current decline at +25 mV, appeared to be greater in capsaicin-responsive neurons (4/7; 42.6±10.9%) compared to neurons insensitive to capsaicin (3/7; 22.2±6.2%). Finally, fitting the I-V curves of the irreversible XE991-sensitive I_{tail} to Boltzmann function gave rise to a G_{max} of 6.5±1.8 nS/pF with $V_{0.5}$ at -38.2±2.9 mV and a slop factor of 7.6±1.0 mV (n=9). The mean normalized activation curve is shown in Fig. 2E (filled circle and solid curve).

Thus, the sustained component of irreversible XE991-sensitive currents recorded in mouse nodose neurons not only exhibits the major biophysical properties characterizing I_M (5, 23), such as substantial activation in subthreshold voltage range, being reversed at E_K, low current density, slow deactivation and activation rates, and lack of inactivation, but also displays pronounced inward rectification at positive voltages. Furthermore, detailed analyses of I_{tail} recordings revealed that the sustained current sensitive to XE991 is essentially I_M in the

voltage range from channel activation threshold to maximal activation potential (-15 mV) under our experimental conditions; to characterize the voltage-dependent activation of I_M over a broader voltage range, however, obtaining the current irreversibly blocked by XE991 is necessary.

We also evaluated the XE991-sensitive current at a more physiological holding potential (-70 mV) in the absence of any other channel blockers. This experimental setting not only facilitates the recording of both I_M and action potentials on the same cell, but also help detect off-target effects of XE991 on other channels, which is important for interpreting correctly the effects of M-channel inhibition by this agent on AP firing in both nodose neurons and terminals. The XE991-sensitive currents were obtained on 8 neurons using the same voltage-clamp protocol as that shown on Fig.2A except that V_h was set at -70 mV. The non-inactivating XE991-sensitive current reached its maximum at -15 mV, so was the I_{tail} elicited upon repolarization to -60 mV (data not shown). The activation parameters, G_{max} (10.2±1.3 nS/pF), $V_{0.5}$ (-38.3±2.1 mV) and k value (7.0±0.5 mV), obtained in cells held at -70 mV are not statistically different from those derived from I_M, defined as the irreversible XE991-sensitive currents recorded with the V_h of -30 mV (P=0.13, 0.44, and 0.16, respectively). The mean normalized activation curves obtained with V_h at -70 mV and -30 mV are almost superimposable (Fig. 2E), confirming that I_M is the major sustained current blocked by XE991 at subthreshold voltages in nodose neurons held at the physiological potential. While holding the neurons at -70 mV, we also noticed that XE991 (10 µM) reduced a fast inward current activated around -45 mV.

Effects of M-channel opener retigabine on I_M in mouse nodose neurons

Figure 3A shows the representative current traces recorded before and after bath application of 10 μM retigabine, and after subsequent addition of 10 μM XE991 in the presence of retigabine. The current traces recorded in the presence of both retigabine and XE991 and in the presence of XE991 alone (after washout of retigabine, not shown for clarity) were not different, indicating that the effects of retigabine on membrane current are mediated by its action on M-channels. The XE991-sensitive currents, defined as I_M, in the absence and presence of retigabine were derived by digital subtractions (Fig. 3A, lower panel). Retigabine significantly increased the amplitude of I_M tail currents (mean I_{in} amplitude: 195±51 *vs.* 146±41 pA, n=7, p=0.02), and markedly reduced the current relaxation rate as indicated by an increased I_{ss}/I_{in} ratio (0.74±0.06 *vs.* 0.11±0.03, p<0.001). Retigabine also increased the amplitude of sustained current at -30 mV and accelerated the activation rate of I_M evoked by depolarization from -60 to -30 mV (mean activation τ: 149±26 ms *vs.* 227±50 ms, p=0.04). The effects of retigabine were readily reversible upon washout (data not shown).

The mean activation curves of I_M obtained in the absence and presence of retigabine are presented in Fig. 3B. Retigabine caused a prominent hyperpolarizing shift of I_M activation ($V_{0.5}$ from -39.2±3.5 mV to -71.0±1.4 mV, p<0.05, Wilcoxon signed rank test) without significant effects on G_{Max} (7.7±2.7 at baseline *vs.* 8.1±2.9 nS/pF with retigabine, p=0.78) or *k* values (7.3±0.9 at baseline *vs.* 9.2±0.5 with retigabine, p=0.06). Although the maximal conductance of M-channel in mouse nodose neurons was not altered by retigabine, the drug increased significantly the channel opening over voltages from -80 to -30 mV with more than 50% of channels being open around the resting potential. These results are consistent with previously reported effects of retigabine on I_M in various cell types (10).

Effects of pharmacologically modulating I_M on resting membrane potentials and spontaneous firing in mouse nodose neurons

Figure 4 shows the typical recordings and pooled data illustrating the effects of retigabine and/or XE991 on the resting potential of mouse nodose neurons. Retigabine (10 μM) hyperpolarized the cells by an averaged 12 mV (from -60.8±0.7 to -72.9±0.6 mV, n=24). This effect was readily reversible upon washing out the drug, or by subsequent application of XE991 suggesting that the retigabine-induced hyperpolarization was mediated via its action on M-channels (Fig. 4A, B). Bath application of XE991 caused a small, but significant membrane depolarization (Fig. 4C, D), even in the presence of retigabine (Fig. 4A,B). Addition of retigabine in the presence of XE991 caused a transient hyperpolarization (Fig. 4C, upper panel), probably due to the opening of originally closed I_M channels which were subsequently blocked by XE991. In support of this idea, second application of retigabine did not cause significant changes in the membrane potential. Similarly, retigabine applied after the cell was stimulated to fire the action potential repetitively for 3-5 mins in the presence of XE991 did not induce membrane hyperpolarization (Fig. 4C, lower panel). The mean value of resting potentials measured at steady-state following application of retigabine in the presence of XE991 is given in Fig. 4D. These results further confirm that retigabine causes membrane hyperpolarization by activating available M-channels. These observations are also in good agreement with the latest finding that the blocking effects of XE991 on KCNQ channels are state-dependent and favor the activated channels (22). Finally, the depolarization caused by XE991 was not reversible, consistent with the irreversible block of I_M by this agent.

Spontaneous AP firing was observed in 3 out of more than 60 mouse nodose neurons examined under current clamp in this study. One example is shown in Fig. 4E. Bath perfusion of retigabine hyperpolarized the membrane and nearly abolished the spontaneous activities. Addition of XE991 in the presence of retigabine reversed the hyperpolarization followed by a persistent AP discharge. The inhibitory effects of opening M-channels on spontaneous AP firings were also observed in the other two neurons.

Effects of pharmacologically modulating I_M on excitability of nodose neurons

To determine further the role of I_M in the regulation of nodose neuron excitability, we have examined the effects of retigabine and XE991 on rheobase, AP threshold, AP numbers in response to suprathreshold stimulation. Retigabine increased the rheobase by an average of 4-fold in 14 cells studied (Fig. 5A and B, left). This is consistent with a large reduction of input resistance around the resting potential of the cells induced by retigabine (from 974±12 to 227±58 MΩ, n=16, p<0.001). XE991 increased significantly the input resistance (from 907±15 to 1297±16MΩ, n=11, p=0.02), but had variable effects on the rheobase: increasing in 8/18 cells, decreasing in 4/18 cells and unchanged in 6/18 cells, resulting in an unchanged mean value compared to baseline (Fig. 5A and B, middle). Similar effects were observed when retigabine was applied in the presence of XE991 or vice versus (Fig. 5A and B, right). The different effects of XE991 on the rheobase among different cells did not seem to be related to the amplitude of I_M measured on the same cells (n=8, correlation coefficient R=0.16) or degree of XE991-induced depolarization (n=18, R=0.09). In contrast to its effect on the rheobase, retigabine did not alter the AP threshold while XE991, paradoxically, increased it regardless whether retigabine was present (Fig. 5C). Reduced AP amplitude (116±4 *vs.* 122±3 mV, n=20, p<0.001) and the peak of

the rate of AP upstroke (147±10 *vs.* 163±9 V/s, n=20, p=0.007) were also observed in the presence of XE991.

The number of APs evoked by 1-sec depolarizing current in mouse nodose neurons increased when the amount of injected current increased from 2-fold to 5-fold rheobase, without further increase at 10-fold rheobase (Figure 5D). Retigabine effectively lowered the AP numbers in response to stimuli of all three intensities,, an effect completely reversible upon washout (Fig. 5D, left). XE991 did not, however, significantly affect the AP firing evoked by suprathreshold stimulations (Fig. 5D, right). We have also examined the effect of retigabine and XE991 on AP firing evoked by a suprathreshold stimulation of the same intensity (1 nA for 1 sec). Again, the AP number was decreased in the presence of retigabine, but not significantly changed by XE991 (Fig. 5E).

Effects of M-channel modulators on excitability of vagal C-fibers innervating the mouse lungs

We next examined whether M-channel activities play a role in regulating the excitability of vagal sensory C-fiber terminals in the mouse lung, key sites for initiation of action potentials. We have previously shown that α,β-MeATP evokes AP discharge in mouse and guinea-pig nodose C-fibers via activation of $P2X_2/P2X_3$ heterotrimeric ion channels (20, 24). In the present study, repetitive applications of 3 μM α,β-meATP activated the mouse nodose C-fibers with similar AP firing (AP numbers: 39±11 and 47±14 for the first and second agonist stimulation, n=10). In fibers pretreated with 10 μM retigabine, however, the agonist failed to evoke any AP in 5/7 fibers and induced only 1 or 2 APs in the other 2 fibers (Fig. 6B). Retigabine also abolished the spontaneous activities observed in 4 fibers and one example is shown in Fig. 6C. Pretreatment of the lungs with 10-30 μM of XE991 prevented the ability of retigabine to abolish

the α,β-meATP-induced AP firing (Fig. 6D), suggesting that retigabine suppressed mouse lung C-fiber excitability via opening the M-channels at the nerve endings. XE991 per se did not increase the excitability of the C-fiber terminals. In fact the average number of APs evoked by 3 and 10 μM α,β-meATP was reduced in the presence of XE991, albeit not in a statistically significant manner (48±24 APs for control *vs.* 24±7 APs with XE991, n=6, p=0.21, and 45±16 APs for control *vs.* 31±7 APs with XE991, n=6, p= 0.19, respectively).

Effects of XE991 on sodium current (I_{Na}) in mouse nodose neurons

Our results show that XE991 tends to inhibit the agonist-evoked AP firing in mouse bronchopulmonary C-fibers, has a variable effect on the rheobase and paradoxically increases the AP threshold in nodose neurons accompanied by a reduction in AP amplitude and in the maximal rate of AP upstroke. We also observed that XE991 reduced a fast inward current by about 25% when nodose neurons were held at -70 mV to record I_M. These findings prompted us to examine whether XE991 has an off-target effect on Na^+ currents, that are critical to AP initiation and conduction, in mouse nodose neurons. We have previously shown that mouse nodose neurons mainly express $Na_V1.7$, $Na_V1.8$ and $Na_V1.9$ (25), and in guinea pig nodose neurons that $Na_V1.7$ mediates the fast TTX-sensitive I_{Na} and $Na_V1.8$ mediates the slower TTX-resistant I_{Na} (26). To evaluate the effects of XE991 on Na^+ currents, the nodose neurons were held at -120 mV and two depolarizing pulses, separated by a 1-sec interval at -70 mV, were applied every 15 seconds to voltages that elicit the maximal I_{Na} (Fig. 7A). In 2 of 4 neurons studied with this protocol, a slower I_{Na} component contributed significantly to the total current. Figure 7 presents the results obtained from a neuron that mainly expressed the fast I_{Na} (Fig. 7B) and from a neuron that had a significant slow component of I_{Na} (Fig. 7C). Bath application of

XE991 significantly reduced the amplitude of total I_{Na} in both cells, with greater effects being found on the currents elicited from -70 mV, a voltage more relevant to physiological conditions. For the neuron shown in Fig. 7C, the fast I_{Na} elicited from -70 mV was largely inhibited by 30 μM XE991, leaving out the slow I_{Na} component. In 3 neurons where the effects of XE991 at both 10 and 30 μM were examined, the total I_{Na} evoked from -120 mV was inhibited by 13±2% and 27±6%, and the current elicited from -70 mV reduced by 31±5% and 53±12% by 10 and 30 μM XE991, respectively. These results reveal a substantial inhibitory effect of XE991 on fast I_{Na} in mouse nodose neurons. Therefore, the effect of this M-channel blocker on neuronal excitability in any given mouse nodose neuron is likely the net effect of opposing actions induced by inhibition of I_M and inhibition of I_{Na}.

Effects of M-channel opener retigabine on irritant gases-induced cough in awake mice

To determine whether activating M-channels at the bronchopulmonary C-fiber terminals inhibits the *in vivo* airway reflex responses, we examined the effects of nebulized retigabine on irritant gases-induced cough in awake mice. Coughs were identified by the three distinct but tightly connected phases of the synchronized changes in both chamber pressure (P_{cham}) and intra-pleural pressure (P_{ip}, Fig. 8A), generated by the initial inspiratory effort followed by chest compression and a forced expiration. Typically, P_{ip} rose sharply to >40 mmHg at the end of the chest-compression. The forced expiration coincided with a detectable cough sound (data not shown). Cough was generally not detected before inhalation challenge (Fig. 8B,C). Both SO_2 and NH_3 inhalation challenges evoked coughs in a concentration-dependent manner ($p<0.01$ between 300 and 600 ppm SO_2; and $p<0.05$ between 0.1% and 0.2% NH_3).

Following retigabine inhalation, cough responses to both low and high concentrations of SO_2 were almost completely blocked (Fig. 8A-C). The inhibitory effect of retigabine on NH_3-evoked coughs was more modest, particularly at higher concentration of NH_3 (43% inhibition, Fig. 8B,C). The anti-tussive effect of retigabine was reproducible as evidenced by similar effects observed when tested on a different day (Fig. 8C). The cough responses to irritant gases were fully recovered 24 hrs-post retigabine treatment indicating absence of desensitization of responses to irritant gases. Furthermore, vehicle of retigabine (isotonic saline) delivered in the same manner did not have any effect on coughs in 2 mice tested (data not shown).

Discussion

This study provided the first evidence that the M-channel activities regulate the excitability of airway vagal afferent C-fibers and the evoked cough responses in mice. The main findings include: (1) the *Kcnq3* is the most prevalent *Kcnq* transcript found in mouse nodose neurons and in lung-specific nodose neurons, and may form functional homotetrameric channels in these cells, (2) I_M contributes to maintaining the negative resting potential in mouse nodose neurons, (3) activation of I_M by retigabine suppresses the excitability of mouse nodose neurons via membrane hyperpolarization and reduced input resistance, and (4) nodose C-fiber terminals innervating the mouse lung express functional M-channels and pharmacologically activating these channels represents a powerful means to inhibit both spontaneous and agonist-evoked AP discharge and to suppress the irritant gases-induced coughing in freely moving mice.

Characterizatics of M-channels in mouse nodose neurons

The M-current in neonatal rat nodose neurons and in baroreceptor neurons of adult rat nodose ganglia has previously been described (16, 21). In this study, we found that I_M in mouse nodose neurons differs from rat nodose I_M in several aspects: (1) the mouse nodose I_M displays a higher voltage sensitivity, has a more negative $V_{1/2}$ (-39 vs. -24 mV) and reached maximal activation at more negative potentials (-15 vs. 0 mV), (2) it exhibits an inward rectification at positive potentials, which is absent in rat nodose I_M, and (3) the same concentration of retigabine produces a larger hyperpolarizing shift of mouse I_M activation curve ($V_{1/2}$ shifted by -32 mV compared to ≤ 15 mV left shift of I-V curves in rats). The different *KCNQ*/K_V7 expression

profiles in rat and mouse nodose neurons likely contribute to this phenotypic difference. It has been reported that positive immunoreactivities for KCNQ2/K_v7.2, KCNQ3/K_v7.3 and KCNQ5/K_v7.5 subunits were detected in all neonatal rat nodose neurons and in beroreceptor terminals of adult rats(16, 21). In mouse nodose neurons (including lung-specific nodose neurons), however, the expression of *Kcnq3* is most prevailing, followed by *Kcnq2* and few neurons express *Kcnq5*. Notably, 50% of mouse *Trpv1*-positive C-fiber neurons express solely *Kcnq3*, and about half of mouse nodose neurons express *Kcnq2* along with *Kcnq3*, most frequently seen in *Trpv1*-negative neurons. Heterologous expression studies have shown that the neuronal KCNQ2-5/K_v7.2-7.5 subunits can form functional homomeric M-channels (27-29), whereas co-expression of KCNQ3 with KCNQ2, KCNQ4 or KCNQ5 subunits usually leads to the formation of heterotetrameric channels that generate larger M-currents (6, 27, 30). These various homomeric and heteromeric KCNQ/M-channels have distinct biophysical and pharmacological properties. For example, the pronounced inward rectification at positive potentials, believed to result from channel inactivation at strong depolarization (28), has been shown to be a characteristic of KCNQ3 or KCNQ5 homomer-mediated whole-cell currents (27-29, 31). Comparative studies on voltage-dependent activation have shown that heterologously expressed KCNQ3/K_V7.3 homomers have a more negative $V_{0.5}$ (-29 to -40 mV) and maximal activation voltages (-30 to -10 mV), as well as a steeper slope (5-6 mV vs. ≥10 mV) than KCNQ2, KCNQ4, KCNQ5 homomeric and KCNQ2/3 heteromeric channels (29, 32-35). Different KCNQ channels also exhibit different sensitivities to retigabine. The same concentration of retigabine (10 μM) caused the largest hyperpolarizing shift of voltage-dependent activation in KCNQ3 homomeric channels, followed by KCNQ2/KCNQ3 and KCNQ3/KCNQ5 heteromeric channels,

and then by KCNQ2 and KCNQ4 homomeric channels expressed in CHO cells (33, 36). The $V_{0.5}$ values in the presence of retigabine found in our mouse nodose neurons (-71 mV) and KCNQ3 homomer-expressing cells (-72 mV)(33) are strikingly similar. Although the degree of retigabine-induced negative shift of I_M activation curve observed in this study (by -32 mV) is less than the -43 mV obtained for KCNQ3 channels in CHO cells, it is significantly larger than those found in other native cells, such as large myelinated fibers of rat sciatic nerve (by -24 mV) where the nodal I_M is mediated by KCNQ2 homomers (37), as well as neocortical myelinated axons (by -29 mV, (38)) and rat sympathetic neurons (by -21 mV, (33)) where I_M is mainly mediated by KCNQ2/3 heteromers. Thus, the electrophysiological characteristics of I_M combined with the unique expression profile of *Kcnq* transcripts found in mouse nodose neurons suggest a contribution of KCNQ3 homotetramers to the functional M-channels in a subset of neurons. This is particularly true in *Trpv1*-positive nodose neurons where *Kcnq3* was the only *Kcnq* subtype expressed in about 50% of the neurons. This inference will remain tentative until additional gene deletion studies are carried out, or until more subtype-selective inhibitors are developed. On the other hand, *Kcnq2* along with *Kcnq3* was expressed in ~30% of *Trpv1*-positive neurons, and in the vast majority of *Trpv1*-negative nodose neurons, consistent with the well established co-localization of KCNQ2 and KCNQ3 subunits at the nodes of Ranvier in both central and pheripheral myelinated fibers(38-40). This expression pattern is also in accord with the less inward rectification of I_M at positive potentials observed in capsaicin-insensitive nodose neurons compared to capsaicin-sensitive ones.

Our finding that KCNQ3/K_V7.3 subunits may form functional homomeric M-channels in mouse nodose neurons seems to be at odds with the general impression that KCNQ3/K_V7.3

homomers do not generate significant currents. Indeed, a few studies have found no detectable M-current in oocytes expressing rat KCNQ3 (41) or CHO cells expressing human KCNQ3 (42, 43). Many other studies have, however, reported substantial M-currents when KCNQ3 was expressed in both oocytes (6, 31) and mammalian cell lines (29, 33-35, 44, 45). In fact, KCNQ3/K_v7.3 expressed very well in mammalian expression systems, particularly in tsA cells, such that reliable studies on TEA- (44) or muscarinic receptor activation-induced (29, 45) inhibition of KCNQ3 currents could be performed. Furthermore, it has been shown that KCNQ3 can traffic to the plasma membrane and target to the key sites (nodes of Ranvier and axon initial segment) of neurons although co-assembly with KCNQ2 increases surface expression of both subunits (46-48). Robust expression of KCNQ3 subunits in nodes of KCNQ2-null sensory neurons has also been reported (39). Therefore, our findings in mouse nodose neurons are not inconsistent with most previously published studies on KCNQ3 channels. Moreover, it may suggest that these channels likely function better in the native environments.

In addition to the two most prevalent compositions of KCNQ transcripts, *Kcnq3* and *Kcnq3* with *Kcnq2*, expressed in mouse nodose neurons and lung-specific neurons, *Kcnq5* or *Kcnq4* was detected along with *Kcnq2* and/or *Kcnq3* in about 10% of the neurons. Whether the cells expressing different composition of KCNQ genes represent functionally distinct subsets of neurons needs further investigation. In this regard, previous studies have revealed that K_v7.4 is expressed in ~ 10% of mouse DRG neurons and their peripheral projections representing a subset of rapidly adapting, low-threshold mechanoreceptors and plays a role in modulating the touch sensitivity (49); whereas K_v7.2 and K_v7.3, but not K_v7.4 or K_v7.5, subunits are expressed in a subset of DRG neurons corresponding to the Down-hair Aδ low-threshold mechanoreceptors

and modulate the mechanosensitivity of D-hairs at their peripheral nerve endings in the skin (50).

M-channel activities regulate mouse nodose neuron and airway C-fiber excitability as well as cough response

Our study showed that I_M started to activate around -65 mV in mouse nodose neurons and reached about 5% of maximal activation at cells' resting potentials. Hence, inhibition of M-channels by XE991 consistently evoked a small but significant depolarization indicating that I_M contributes to setting the resting potential in mouse nodose neurons. Opening M-channel by retigabine caused an averaged 12-mV hyperpolarization and profoundly decreased excitability in mouse nodose neurons as evidenced by a more than 4-foled increase in the rheobase; a markedly reduction in evoked AP numbers; and an abolition in spontaneous AP firing. Our results also showed that retigabine reduced the input resistance at resting potentials without altering the AP threshold, suggesting that membrane hyperpolarization and reduced input resistance are the major mechanisms underlying the retigabine effects in our cells. In accordance with the findings in the cell soma, applying retigabine to the receptive field of nodose C-fibers in the mouse lungs strongly reduced the agonist-evoked AP discharge, and abolished the spontaneous activities. These effects were prevented by pretreatment with XE991, indicating that functional KCNQ/K_v7/M-channels are present in the nodose C-fiber terminals where their activation effectively suppresses AP generation.

Although XE991 completely reversed or prevented the inhibitory effects of retigabine on AP discharge in both mouse nodose neurons and C-fiber terminals, an excitatory effect of XE991 *per se* was not observed. In fact, we found that XE991 caused a slight increase in AP

threshold and had a tendency to reduce AP discharge at nodose C-fiber terminals in the lungs. These observations are at odds with the repetitive AP firing induced by focal puff application of XE991 in rat lumbar DRG neurons (51) and with the finding that XE991 modestly increased afferent firing in response to noxious bowel distension in mouse distal colons (17). However, the absence of effects on AP firing properties in mouse sympathetic neurons (52) and an increase in the pressure threshold for rat baroreceptor discharge (16) by XE991 have also been reported. Furthermore, recordings in a skin-saphenous nerve preparation have revealed variable effects of XE991(53, 54). Our finding that XE991 significantly inhibited the fast I_{Na} in mouse nodose neurons has not been previously reported and may be relevant to this discussion. We previously demonstrated that inhibition of the fast I_{Na}, even in neurons that expressed a large slow TTX-resistant I_{Na}, substantially increased the amount of current needed to evoke an AP in guinea-pig nodose and jugular neurons (26). Therefore, the possible excitatory effect of blocking I_M by XE991 in our mouse nodose neurons and terminals may have been offset by XE991-induced I_{Na} inhibition. Accordingly, XE991 may not be an ideal compound to evaluate the influence of blocking M-current on nerve excitability, at least in the mouse vagal sensory system.

Consistent with its inhibitory effect on action potential generation in nodose C-fibers terminating in the lungs, retigabine effectively suppressed irritant gases-evoked coughing in awake mice. Mechanistically, how inhaled SO_2 and NH_3 activates airway sensory afferents and elicits coughs is unclear. The hydrophilic properties of SO_2 suggest it can readily dissolve in the lining fluid covering the mucosa of the respiratory tract and lower the pH, which in turn can activate TRPV1 and acid-sensing ion channels (55, 56). On the other hand, NH_3 can rapidly

diffuse across plasma membrane causing intracellular alkalization which has been shown to activate TRPV1 and TRPA1 (55, 57). Activation of these ion channels is known to cause depolarization and activation of airway vagal afferents, thereby triggering a series of reflex responses including coughs(19). Opening M-channels by retigabine may counteract these depolarizing forces (regardless of the types of the ion channels involved) and make the sensory fibers much less excitable by hyperpolarizing the neurons toward E_K and reducing input resistance, thereby preventing coughs from the irritant gas stimulation. Although retigabine inhalation inhibits both SO_2- and NH_3-evoked coughs, it appears to be less effective for high concentration of NH_3-induced response. It is tempting to speculate that this may be related to the intracellular alkalization caused by NH_3 since pH is known to modulate the gating of numbers of ion channels. It has been shown that intracellular alkalization reduced the KCNQ1/KCNE1-meadiated I_{Ks} current (58). If the same happened to the M-channels in mouse airway vagal afferents it may offset part of retigabine effects. Moreover, in addition to activating TRPV1 and TRPA1 channels, increase in the intracellular pH has been shown to enhance depolarizing N-type Ca^{2+} current (59) and I_h current (60), thus further favoring membrane depolarization.

Therapeutic potential

Increases vagal C-fiber activity can contribute to the reflex bronchospasm and secretions that compromise lung function in asthma and COPD. In addition, inappropriate vagal sensory nerve stimulation can lead to subacute, and in some cases chronic coughing, as well as sensations of dyspnea that are ill-matched to lung function (19). Particularly, chronic cough that affects about 10% of population has very limited treatment options(61). Our results

showed that local activation of M-channels significantly inhibits the excitability of vagal C-fibers innervating mouse lungs and suppresses the cough response to inhaled irritant gases in freely moving mice. If these findings are also observed in humans, the M-channel would be a rational therapeutic target for inflammatory airway diseases. In support of this idea, a recent study has shown that gapapentin, a neuromodulator previously found effective for treatment of refractory chronic cough in patients(61), potently activates M-channels composed of KCNQ3, KCNQ5 homomers or KCNQ2/3 heteromers (62). Moreover, airway smooth muscle cells also express functional KCNQ/K_v7 channels, and activating these channels by flupirtine or retigabine has been shown to attenuate the histamine-induced constriction of human airways (63) and relax the muscarinic-evoked airway contraction in rodents (64, 65). Therefore, a topical (inhaled) formulation of an M-channel activator could be a unique strategy to both inhibit the vagal C-fiber hyperactivity and dilate the bronchi with minimal unwanted central or peripheral side effects.

Methods

Labeling and isolation of nodose neurons

In some studies, the bronchopulmonary afferent neurons were retrogradely labeled using DiI (1,1'-dioctadecyl-3,3,3',3'-tetramethylindocarbocyanine Perchlorate; DiC18(3); Molecular Probes/Invitrogen, Eugene, OR, USA) instilled into the tracheal lumen of anesthetized mice 5-9 days before experiments. The distribution of dye in the lungs, but not in trachea or esophagus, was verified at the time the animals were sacrificed for cell isolation.

Mice were killed by CO_2 inhalation. Both sides of jugular/nodose ganglia were dissected and cleared of adhering connective tissues. The lower 2/3 of ganglia (primarily nodose) were cut out for subsequent enzymatic digestion at 37°C using type 1A collagenase (2mg/ml) and dispase II (2mg/ml). The isolated nodose neurons were plated onto poly-D-lysine/laminin-coated coverslips and kept at 37°C in L-15 medium containing 10% of fetal bovine serum for use within 8 hours for cell collection or within 24 hours for patch clamp recordings.

Single-cell RT-PCR assay

Single unlabeled or retrogradelly labeled nodose neurons identified under a fluorescence microscope were collected into a PCR tube (one cell per tube) containing 1 µl RNAse Inhibitor (RNAseOUT, 2 U/µl) two hours after isolation and immediately snap frozen. A sample of the bath solution from the vicinity of a neuron was collected from each coverslip for no-template experiments (bath control).

The first strand cDNA was synthesized using the SuperScript III First-Strand Synthesis System for RT-PCR (Cat#18080, Invitrogen, Carlsbad, CA, USA) according to the manufacturer's

recommendations. 1.2 µl of synthesized cDNA (or RNA control and bath control) was used for PCR amplification (50 cycles) for mouse *Trpv1*, *P2rx2*, *Kcnq2-5* using custom-synthesized primers (Sigma-Aldrich) (Table 1) and the HotStar Taq Poymerase Kit (Qiagen) in a final volume of 20 µl. PCR products were visualized in ethidum bromide-stained 1.5% agarose gels.

The Kcnq genes were first screened in mouse nodose ganglia with cDNA synthesized from total RNA isolated from mouse brain, heart and/or skeletal muscle as positive controls. *Kcnq1*, abundant in the heart, was not detected in nodose ganglia. Hence, only *Kcnq2-5* that were found in whole ganglia were examined in the single-neuron PCR assay.

Patch clamp recording and analysis

Amphotericin B-perforated whole-cell patch clamp technique was employed to record the membrane potential and M-currents in nodose neurons at room temperature under current-clamp and voltage-clamp mode, respectively, using an Axopatch 200B amplifier interfaced with Axon Digidata 1550A and driven by pCLAMP 10 software (Molecular Devices, Sunnyvale, CA, USA). Membrane currents were sampled at 5-10 kHz and filtered at 2-5 kHz. Bath solution contained (mM): NaCl 136, KCl 5.4, $MgCl_2$ 1, $CaCl_2$ 1, HEPES 10 and glucose 10 (pH 7.35 with NaOH). To record M-currents with a holding potential of -30 mV, 1 mM CsCl was added to block HCN currents. Pipette solution contained (mM): KCl 20, K-gluconate 125 and HEPES 10 (pH 7.2 with KOH). Freshly prepared amphotericin B was added to the pipette solution (300 µg/ml) before experiments. The junction potential (-14.7 mV estimated using Clampex calculator) was corrected.

Conventional whole-cell patch clamp technique was used to record Na^+ currents (I_{Na}). Bath solution contained (mM): choline-Cl 126, NaCl 10, CsCl 3, TEA-Cl 5, $MgCl_2$ 1, $CaCl_2$ 1, $CdCl_2$ 0.1, HEPES 10 and glucose 10 (pH 7.35 with CsOH). Pipette solution contained (mM): CsF 140, NaCl 10, $MgCl_2$ 1, $CaCl_2$ 0.1, EGTA 1.1 and HEPES 10 (pH 7.2 with CsOH). The current was sampled at 50 kHz and filtered at 10 kHz. The effect of XE991 on I_{Na} was evaluated 8 to 10 minutes after the whole-cell formation when the current become relatively stable. For all voltage-clamp experiments, the cell capacitance and series resistance (80%) were compensated electronically.

Patch clamp recordings were analyzed using Clampfit 10. The steady-state activation of I_M was assessed by measuring tail currents (I_{tail}) at -60 mV following long voltage steps to different potentials. The amplitude of I_{tail} was measured at the peak after correcting for the leak current if necessary. To obtain the activation parameters, data points were fitted to the Boltzmann function for each cell: $I= G_{max}/(1+\exp(-(V_m - V_{0.5})/k))$, or $I/I_{max} = G_{max}/(1+\exp(-(V_m - V_{0.5})/k))$ for normalized activation curves, where G_{max} is maximal conductance, V_m membrane potential, $V_{0.5}$ voltage at which 50% of activation occurs, and *k* the slope factor. The input resistance was calculated by dividing the voltage step (from -70 to -60 mV) by sustained current measured at the end of voltage pulse. The rheobase was measured as the least amount of depolarizing current (100 ms) needed to evoke a single AP. The AP threshold was measured by differentiating the AP voltage with respect to time (dV/dt) and defined as the voltage at which the deflection for dV/dt is greater than zero. The AP amplitude was measure as the difference between the peak of upstroke and the resting potential. The peak of the rate of AP upstroke was measured as the positive peak of dV/dt.

Isolated perfused nerve-lung preparation and extracellular recording

Mice were killed by CO_2 inhalation and exsanguination. The blood from the pulmonary circulation was flushed out by injecting through the right heart 10 ml of Krebs bicarbonate buffer (KBS) composed of (mM): NaCl, 118; KCl, 5.7; NaH_2PO_4, 1.0; $MgSO_4$, 1.2; $CaCl_2$, 1.9; $NaHCO_3$, 25.0; dextrose, 11.1; and gassed with 95 % O_2-5 % CO_2, pH 7.4. The airways and lungs with intact right-side extrinsic vagal innervations (including right jugular-nodose ganglia complex, JNC) were dissected and the tissue was pinned in a small Sylgard-lined Perspex chamber. The right JNC along with the rostral-most vagi were pulled through a small hole into an adjacent chamber for extracellular recording. The hole was then sealed with Vaseline so that the recording chamber and lungs are perfused separately (see Fig. 6A). A piece of PE60 tubing was inserted into the trachea and connected to the infusion pump for continuous perfusion with KBS (35–37 °C, 2 ml/min) of the lungs. Short cuts (< 1 mm deep, 6–10 per lobe) were made on the lung surface to allow exit of the perfusate.

Extracellular recordings of single unit activities were performed in nodose ganglion (lower 2/3 of JNC) using an aluminosilicate glass microelectrode filled with 3 M sodium chloride (electrode resistance ˜2 MΩ). The signal was amplified (Microelectrode AC amplifier 1800, A-M Systems), filtered (low cut off, 0.3 kHz; high cut off, 1 kHz), and stored in the computer for offline analyses using the software NerveOfIt (sampling frequency 33 kHz, PHOCIS, Baltimore, MD, USA). The receptive field was identified using a concentric stimulation electrode (100 V, 0.5 ms, 1 Hz) sequentially positioned at different places on the surface of the lung lobes. When the evoked APs were recorded, the tissue was probed with a mechanical probe (von Frey hair, 60–1800 mN). The mechanosensitive receptive field was identified when the mechanical stimulus

evoked a burst of action potentials. Conduction velocity was calculated by dividing the distance along the nerve pathway by the time between the stimulus artifact and the AP evoked by electrical stimulation of the mechanosensitive receptive field. In this study, only the fibers conducting in the C-fiber range (<1 m/s) were used.

α,β-methylene-ATP (α,β-MeATP) was administered to the lung by adding a 1-ml bolus of KBS containing the appropriate concentration of the agonist to the tracheal perfusion. When the effects of XE991 or retigbine on agonist-induced AP discharge were examined, the KBS containing the drugs was given through tracheal perfusion for 30 mins before the second bolus of agonist was applied.

Cough measurements in awake mice

The irritant gas-induced cough in awake free-moving mice was measured as previously described (66). Briefly, mice moved freely in a plexiglass recording chamber (volume 160 ml). Room air was drawn through the chamber at a constant flow rate (300 ml/min). The CO_2 concentration and temperature of the outlet air were continuously monitored (~0.6% and ~24ºC, respectively, at steady-state). To identify cough reliably in moving mice with inherently unstable breathing, a telemetry sensor (Data Sciences International model PA-C10, St. Paul, MN) was surgically implanted in the intra-pleural space to measure the intra-pleural pressure (P_{ip}) directly, in addition to the continuously recorded pressure of the chamber (P_{cham}) by a pressure transducer (Biopac model TSD160A, Goleta, CA). Audio and video signals of the mouse movements were also recorded. Prior to experiments, the mouse was placed in the recording chamber for >30 min for adaptation. During the inhalation challenge, a gas mixture of SO_2 or NH_3 was drawn into the chamber (replacing room air) at the same flow rate (300 ml/min) for 5

min. All signals were recorded before, during and after each inhalation challenge, each for a 5-min duration.

The reason cough was determined not only by the recording chamber pressure (change in respiratory flow) and the intra-thoracic pressure, but also by simultaneous audio-video recording of the animal's motion and action, was that it allowed us to identify coughs and also to distinguish them from sneezes, sniffs and other respiratory actions. We did observe sneeze triggered occasionally in the early response to inhaled irritant gases such as SO2 in awake mice, though they disappeared completely during the recovery from exposure to SO2. Furthermore, sneezes typically did not generate the peak intra-thoracic pressure (recorded by telemetry sensor) greater than 40 mmHg; and the sound generated by sneeze was not as distinct as that by cough. As such, sneezes were not included in our data analysis of cough response.

Two concentrations of SO_2 (300 and 600 ppm) and NH_3 (0.1 and 0.2 %) balanced in air were tested in each animal. At least 30 min was allowed for a full recovery between two consecutive challenges. The control (without retigabine) experiments were repeated 3 times on 3 separate days in each mouse. The effect of retigabine on cough sensitivity was tested at least 24 hours after completion of control experiments and repeated once 1-2 days later to test the reproducibility. Retigabine aerosol (250 μM) were generated by a ultrasonic nebulizer (Lumiscope 6610, Lumiscope, East Brunswick, NJ) and administered to the mouse in an exposure chamber for 15 min. 5 min later the inhalation challenges were carried out. The sequence of SO_2 and NH_3 as well as the high/low concentrations of each gas was alternated between days in each mouse to achieve a balanced design.

S*tatistics*

All statistical analyses were performed using SigmaPlot software. Pooled data are expressed as mean ± SEM. The statistical significance of differences between two means was determined by using either paired or unpaired Student's *t*-test, as appropriate. In the cases that the normality test failed, Wilcoxon signed rank test or Mann-Whitney rank sum test was used as appropriate. The significance of differences between multiple means was evaluated by one way repeated measures ANOVA. The significance of difference between two or multiple means and with different levels of treatment was evaluated by two way repeated measures ANOVA. Holm-Sidak or Fisher's test as a *post hoc* analysis was performed for multiple pairwise comparisons. A P value less than 0.05 was considered significant.

Study approval

All experiments carried out were approved by IACUC of Johns Hopkins University and University of Kentucky. Male C57BL/6J mice (6-14 weeks, from Jackson Laboratory) were used in this study.

Author contributions:

HS designing research studies, conducting experiments, analyzing data and writing the manuscript; AHL, FR, MJP and SM conducting experiments and analyzing data; LYL designing research studies and analyzing data; BJU designing research studies and writing the manuscript.

Acknowledgements:

This study was supported by R01 HL122228 and U01 AI123832

References

1. Lehman A, et al. Loss-of-Function and Gain-of-Function Mutations in KCNQ5 Cause Intellectual Disability or Epileptic Encephalopathy. *American journal of human genetics.* 2017;101(1):65-74.
2. Maljevic S, Wuttke TV, Seebohm G, and Lerche H. KV7 channelopathies. *Pflugers Archiv : European journal of physiology.* 2010;460(2):277-88.
3. Brown DA, and Adams PR. Muscarinic suppression of a novel voltage-sensitive K+ current in a vertebrate neurone. *Nature.* 1980;283(5748):673-6.
4. Brown BS, and Yu SP. Modulation and genetic identification of the M channel. *Progress in biophysics and molecular biology.* 2000;73(2-4):135-66.
5. Brown DA, and Passmore GM. Neural KCNQ (Kv7) channels. *British journal of pharmacology.* 2009;156(8):1185-95.
6. Schroeder BC, Kubisch C, Stein V, and Jentsch TJ. Moderate loss of function of cyclic-AMP-modulated KCNQ2/KCNQ3 K+ channels causes epilepsy. *Nature.* 1998;396(6712):687-90.
7. Biervert C, et al. A potassium channel mutation in neonatal human epilepsy. *Science.* 1998;279(5349):403-6.
8. Charlier C, et al. A pore mutation in a novel KQT-like potassium channel gene in an idiopathic epilepsy family. *Nature genetics.* 1998;18(1):53-5.
9. Hansen HH, et al. Kv7 channels: interaction with dopaminergic and serotonergic neurotransmission in the CNS. *The Journal of physiology.* 2008;586(7):1823-32.
10. Gunthorpe MJ, Large CH, and Sankar R. The mechanism of action of retigabine (ezogabine), a first-in-class K+ channel opener for the treatment of epilepsy. *Epilepsia.* 2012;53(3):412-24.
11. Large CH, et al. The spectrum of anticonvulsant efficacy of retigabine (ezogabine) in animal models: implications for clinical use. *Epilepsia.* 2012;53(3):425-36.
12. Rivera-Arconada I, Roza C, and Lopez-Garcia JA. Enhancing m currents: a way out for neuropathic pain? *Frontiers in molecular neuroscience.* 2009;2:10.
13. Du X, Gao H, Jaffe D, Zhang H, and Gamper N. M-type K(+) channels in peripheral nociceptive pathways. *British journal of pharmacology.* 2018;175(12):2158-72.
14. Linley JE, Rose K, Ooi L, and Gamper N. Understanding inflammatory pain: ion channels contributing to acute and chronic nociception. *Pflugers Archiv : European journal of physiology.* 2010;459(5):657-69.
15. Wu Z, et al. Activation of KCNQ Channels Suppresses Spontaneous Activity in Dorsal Root Ganglion Neurons and Reduces Chronic Pain after Spinal Cord Injury. *Journal of neurotrauma.* 2017;34(6):1260-70.
16. Wladyka CL, Feng B, Glazebrook PA, Schild JH, and Kunze DL. The KCNQ/M-current modulates arterial baroreceptor function at the sensory terminal in rats. *The Journal of physiology.* 2008;586(3):795-802.
17. Peiris M, et al. Peripheral KV7 channels regulate visceral sensory function in mouse and human colon. *Molecular pain.* 2017;13:1744806917709371.
18. Hirano K, et al. Kv7.2-7.5 voltage-gated potassium channel (KCNQ2-5) opener, retigabine, reduces capsaicin-induced visceral pain in mice. *Neuroscience letters.* 2007;413(2):159-62.
19. Mazzone SB, and Undem BJ. Vagal Afferent Innervation of the Airways in Health and Disease. *Physiological reviews.* 2016;96(3):975-1024.
20. Nassenstein C, et al. Phenotypic distinctions between neural crest and placodal derived vagal C-fibres in mouse lungs. *The Journal of physiology.* 2010;588(Pt 23):4769-83.
21. Wladyka CL, and Kunze DL. KCNQ/M-currents contribute to the resting membrane potential in rat visceral sensory neurons. *The Journal of physiology.* 2006;575(Pt 1):175-89.

22. Greene DL, Kang S, and Hoshi N. XE991 and Linopirdine Are State-Dependent Inhibitors for Kv7/KCNQ Channels that Favor Activated Single Subunits. *The Journal of pharmacology and experimental therapeutics.* 2017;362(1):177-85.
23. Robbins J. KCNQ potassium channels: physiology, pathophysiology, and pharmacology. *Pharmacology & therapeutics.* 2001;90(1):1-19.
24. Kwong K, Kollarik M, Nassenstein C, Ru F, and Undem BJ. P2X2 receptors differentiate placodal vs. neural crest C-fiber phenotypes innervating guinea pig lungs and esophagus. *American journal of physiology Lung cellular and molecular physiology.* 2008;295(5):L858-65.
25. Wang J, et al. Distinct and common expression of receptors for inflammatory mediators in vagal nodose versus jugular capsaicin-sensitive/TRPV1-positive neurons detected by low input RNA sequencing. *PloS one.* 2017;12(10):e0185985.
26. Kollarik M, et al. Different role of tetrodotoxin-sensitive voltage-gated sodium channel (NaV1) subtypes in action potential initiation and conduction in vagal airway nociceptors. *The Journal of physiology.* 2018.
27. Lerche C, et al. Molecular cloning and functional expression of KCNQ5, a potassium channel subunit that may contribute to neuronal M-current diversity. *The Journal of biological chemistry.* 2000;275(29):22395-400.
28. Schroeder BC, Hechenberger M, Weinreich F, Kubisch C, and Jentsch TJ. KCNQ5, a novel potassium channel broadly expressed in brain, mediates M-type currents. *The Journal of biological chemistry.* 2000;275(31):24089-95.
29. Selyanko AA, et al. Inhibition of KCNQ1-4 potassium channels expressed in mammalian cells via M1 muscarinic acetylcholine receptors. *The Journal of physiology.* 2000;522 Pt 3:349-55.
30. Kubisch C, et al. KCNQ4, a novel potassium channel expressed in sensory outer hair cells, is mutated in dominant deafness. *Cell.* 1999;96(3):437-46.
31. Yang WP, et al. Functional expression of two KvLQT1-related potassium channels responsible for an inherited idiopathic epilepsy. *The Journal of biological chemistry.* 1998;273(31):19419-23.
32. Selyanko AA, Hadley JK, and Brown DA. Properties of single M-type KCNQ2/KCNQ3 potassium channels expressed in mammalian cells. *The Journal of physiology.* 2001;534(Pt 1):15-24.
33. Tatulian L, Delmas P, Abogadie FC, and Brown DA. Activation of expressed KCNQ potassium currents and native neuronal M-type potassium currents by the anti-convulsant drug retigabine. *The Journal of neuroscience : the official journal of the Society for Neuroscience.* 2001;21(15):5535-45.
34. Roche JP, et al. Antibodies and a cysteine-modifying reagent show correspondence of M current in neurons to KCNQ2 and KCNQ3 K+ channels. *British journal of pharmacology.* 2002;137(8):1173-86.
35. Li Y, Gamper N, and Shapiro MS. Single-channel analysis of KCNQ K+ channels reveals the mechanism of augmentation by a cysteine-modifying reagent. *The Journal of neuroscience : the official journal of the Society for Neuroscience.* 2004;24(22):5079-90.
36. Wickenden AD, Zou A, Wagoner PK, and Jegla T. Characterization of KCNQ5/Q3 potassium channels expressed in mammalian cells. *British journal of pharmacology.* 2001;132(2):381-4.
37. Schwarz JR, et al. KCNQ channels mediate IKs, a slow K+ current regulating excitability in the rat node of Ranvier. *The Journal of physiology.* 2006;573(Pt 1):17-34.
38. Battefeld A, Tran BT, Gavrilis J, Cooper EC, and Kole MH. Heteromeric Kv7.2/7.3 channels differentially regulate action potential initiation and conduction in neocortical myelinated axons. *The Journal of neuroscience : the official journal of the Society for Neuroscience.* 2014;34(10):3719-32.
39. King CH, Lancaster E, Salomon D, Peles E, and Scherer SS. Kv7.2 regulates the function of peripheral sensory neurons. *The Journal of comparative neurology.* 2014;522(14):3262-80.

40. Pan Z, et al. A common ankyrin-G-based mechanism retains KCNQ and NaV channels at electrically active domains of the axon. *The Journal of neuroscience : the official journal of the Society for Neuroscience.* 2006;26(10):2599-613.
41. Wang HS, et al. KCNQ2 and KCNQ3 potassium channel subunits: molecular correlates of the M-channel. *Science.* 1998;282(5395):1890-3.
42. Wickenden AD, Yu W, Zou A, Jegla T, and Wagoner PK. Retigabine, a novel anti-convulsant, enhances activation of KCNQ2/Q3 potassium channels. *Molecular pharmacology.* 2000;58(3):591-600.
43. Main MJ, et al. Modulation of KCNQ2/3 potassium channels by the novel anticonvulsant retigabine. *Molecular pharmacology.* 2000;58(2):253-62.
44. Hadley JK, et al. Differential tetraethylammonium sensitivity of KCNQ1-4 potassium channels. *British journal of pharmacology.* 2000;129(3):413-5.
45. Shapiro MS, et al. Reconstitution of muscarinic modulation of the KCNQ2/KCNQ3 K(+) channels that underlie the neuronal M current. *The Journal of neuroscience : the official journal of the Society for Neuroscience.* 2000;20(5):1710-21.
46. Schwake M, Pusch M, Kharkovets T, and Jentsch TJ. Surface expression and single channel properties of KCNQ2/KCNQ3, M-type K+ channels involved in epilepsy. *The Journal of biological chemistry.* 2000;275(18):13343-8.
47. Chung HJ, Jan YN, and Jan LY. Polarized axonal surface expression of neuronal KCNQ channels is mediated by multiple signals in the KCNQ2 and KCNQ3 C-terminal domains. *Proceedings of the National Academy of Sciences of the United States of America.* 2006;103(23):8870-5.
48. Rasmussen HB, et al. Requirement of subunit co-assembly and ankyrin-G for M-channel localization at the axon initial segment. *Journal of cell science.* 2007;120(Pt 6):953-63.
49. Heidenreich M, et al. KCNQ4 K(+) channels tune mechanoreceptors for normal touch sensation in mouse and man. *Nature neuroscience.* 2011;15(1):138-45.
50. Schutze S, Orozco IJ, and Jentsch TJ. KCNQ Potassium Channels Modulate Sensitivity of Skin Down-hair (D-hair) Mechanoreceptors. *The Journal of biological chemistry.* 2016;291(11):5566-75.
51. Barkai O, et al. The Role of Kv7/M Potassium Channels in Controlling Ectopic Firing in Nociceptors. *Frontiers in molecular neuroscience.* 2017;10:181.
52. Romero M, Reboreda A, Sanchez E, and Lamas JA. Newly developed blockers of the M-current do not reduce spike frequency adaptation in cultured mouse sympathetic neurons. *The European journal of neuroscience.* 2004;19(10):2693-702.
53. Vetter I, et al. Amplified cold transduction in native nociceptors by M-channel inhibition. *The Journal of neuroscience : the official journal of the Society for Neuroscience.* 2013;33(42):16627-41.
54. Passmore GM, et al. Functional significance of M-type potassium channels in nociceptive cutaneous sensory endings. *Frontiers in molecular neuroscience.* 2012;5:63.
55. Dhaka A, et al. TRPV1 is activated by both acidic and basic pH. *The Journal of neuroscience : the official journal of the Society for Neuroscience.* 2009;29(1):153-8.
56. Canning BJ. Afferent nerves regulating the cough reflex: mechanisms and mediators of cough in disease. *Otolaryngologic clinics of North America.* 2010;43(1):15-25, vii.
57. Fujita F, et al. Intracellular alkalization causes pain sensation through activation of TRPA1 in mice. *The Journal of clinical investigation.* 2008;118(12):4049-57.
58. Unsold B, et al. KCNE1 reverses the response of the human K+ channel KCNQ1 to cytosolic pH changes and alters its pharmacology and sensitivity to temperature. *Pflugers Archiv : European journal of physiology.* 2000;441(2-3):368-78.

59. Kiss L, and Korn SJ. Modulation of N-type Ca2+ channels by intracellular pH in chick sensory neurons. *Journal of neurophysiology.* 1999;81(4):1839-47.
60. Munsch T, and Pape HC. Modulation of the hyperpolarization-activated cation current of rat thalamic relay neurones by intracellular pH. *The Journal of physiology.* 1999;519 Pt 2:493-504.
61. Ryan NM, Birring SS, and Gibson PG. Gabapentin for refractory chronic cough: a randomised, double-blind, placebo-controlled trial. *Lancet.* 2012;380(9853):1583-9.
62. Manville RW, and Abbott G. Gabapentin is a potent activator of KCNQ3 and KCNQ5 potassium channels. *Molecular pharmacology.* 2018.
63. Brueggemann LI, et al. Kv7 potassium channels in airway smooth muscle cells: signal transduction intermediates and pharmacological targets for bronchodilator therapy. *American journal of physiology Lung cellular and molecular physiology.* 2012;302(1):L120-32.
64. Evseev AI, et al. Functional effects of KCNQ K(+) channels in airway smooth muscle. *Frontiers in physiology.* 2013;4:277.
65. Brueggemann LI, et al. KCNQ (Kv7) potassium channel activators as bronchodilators: combination with a beta2-adrenergic agonist enhances relaxation of rat airways. *American journal of physiology Lung cellular and molecular physiology.* 2014;306(6):L476-86.
66. Zhang C, Lin RL, Hong J, Khosravi M, and Lee LY. Cough and expiration reflexes elicited by inhaled irritant gases are intensified in ovalbumin-sensitized mice. *American journal of physiology Regulatory, integrative and comparative physiology.* 2017;312(5):R718-R26.

Figures and Figure legends

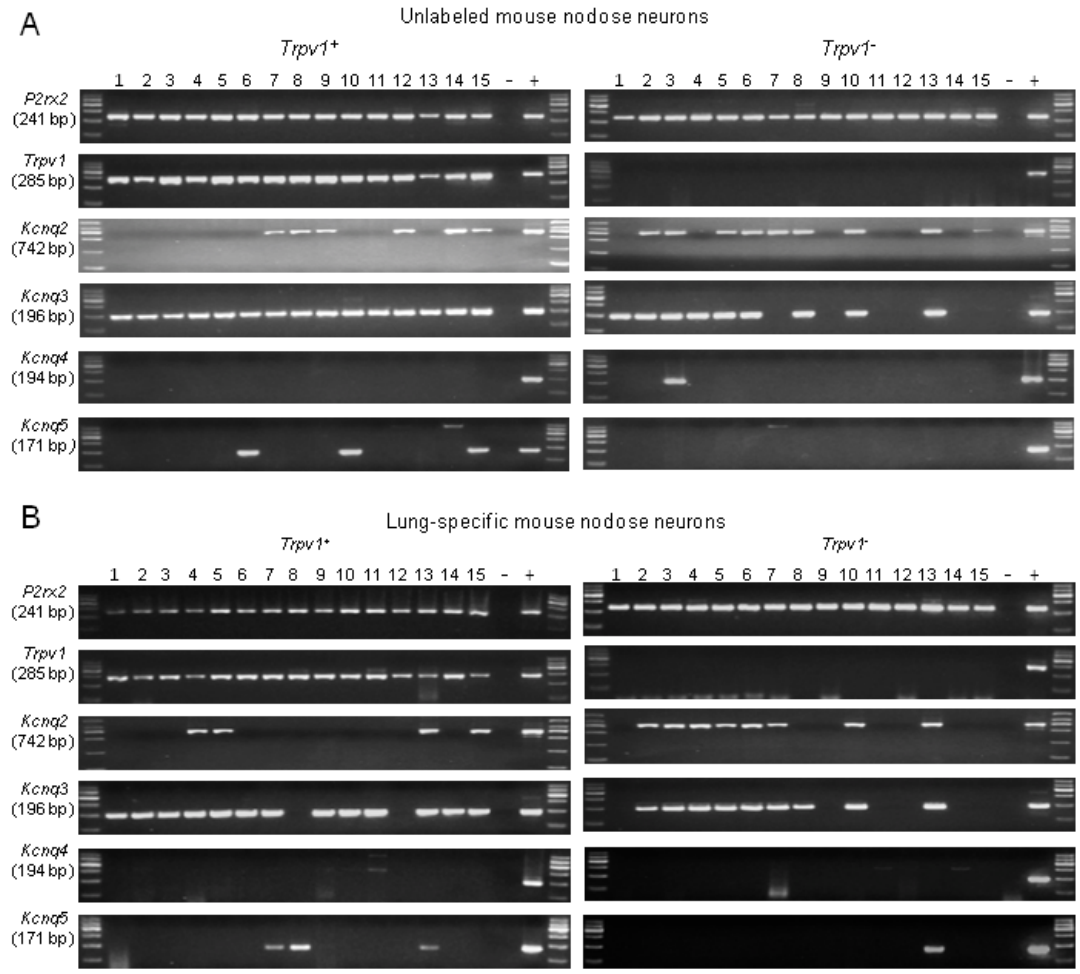

Figure 1. Expression profile of *Kcnq* transcripts in unlabeled mouse nodose neurons (**A**) and lung-specific nodose neurons (**B**). Each lane (numbered on the top of gel images) shows results obtained from one neuron. -: negative control; +: positive control. Mid range DNA ladder was used for *Kcnq2* amplicon and the bands read 2000, 1000, 750, 500, 250 and 100 bp from the top. 100 bp ladder was used for amplicons of other genes and the bands read 600 to 100 bp from the top with 100 bp decrement. The size of amplicons is given below the gene name. *Trpv1*$^{+}$: *Trpv1*-positive; *Trpv1*$^{-}$: *Trpv1*-negative.

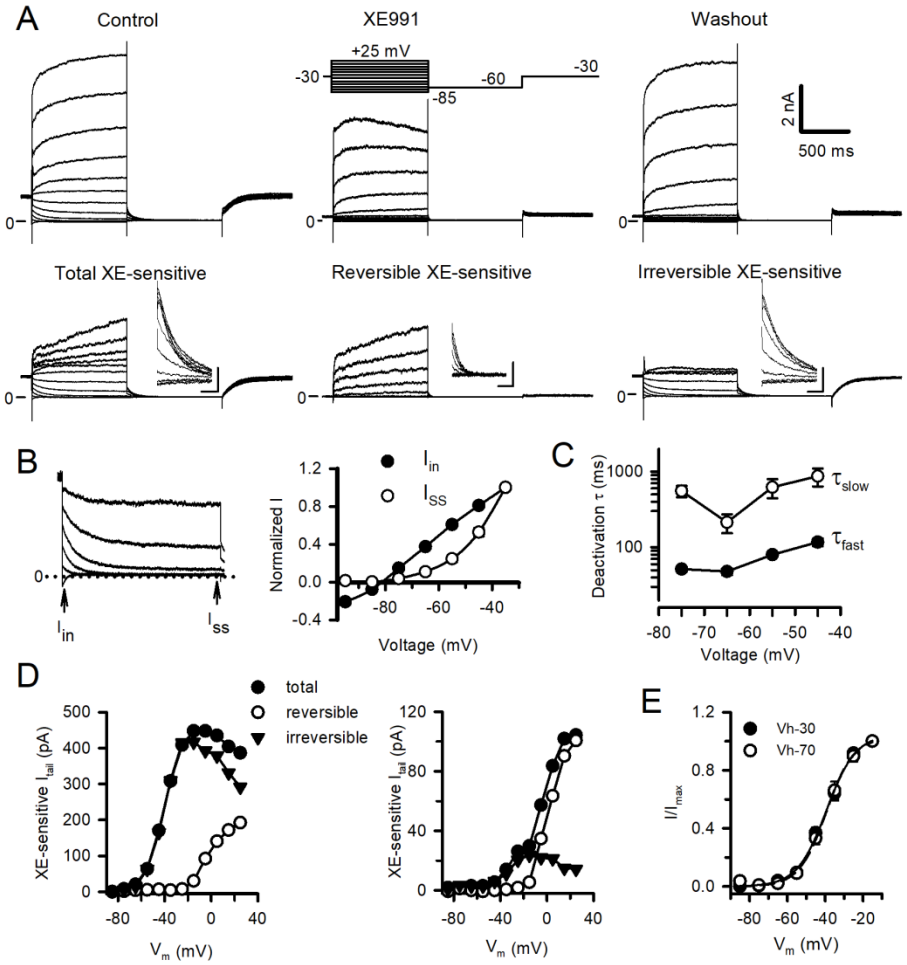

Figure 2. Characterization of I_M in mouse nodose neurons. **A.** Representative current recordings obtained from one of 9 neurons in the absence and presence of 10 µM XE991, and after washout of the drug (*upper row*) using the voltage-clamp protocol shown in inset, and XE991-sensitive currents obtained by digital subtraction (*lower row*, see text). Tail currents (I_{tail}) in the lower panels are shown at expanded scales in the inset. Calibration bars: 100 pA and 50 ms. **B.** *left:* The irreversible XE991-sensitive currents evoked by hyperpolarization from V_h to -85 through -35 mV are re-plotted from panel **A** to illustrate how the instantaneous (I_{in}) and sustained currents (I_{ss}) were measured. *right:* Mean normalized I-V curves of I_{in} and I_{ss} (n=9). **C.** Semi-logarithmic plot of deactivation time constants (τ) of irreversible XE991-sensitive currents recorded during the first voltage clamp pulses against voltages (n=5). **D.** The amplitudes of total, reversible and irreversible XE991-sensitive I_{tail} obtained from the neuron shown on panel A (*left*) and from another neuron (*right*), respectively, are plotted against the voltages of prior voltage steps (V_m). **E.** Mean normalized activation curves for the irreversible XE991-sensitive current obtained with the V_h at -30 mV (n=9) and for the XE991-sensitive current recorded with the V_h at -70 mV (n=8). The solid and dashed curves represent the fit of data points to the Boltzmann function.

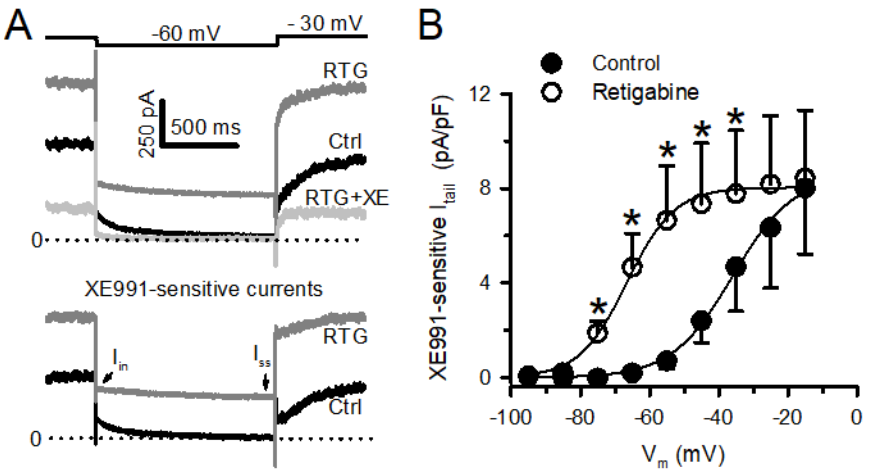

Figure 3. Effects of retigabine on I_M in mouse nodose neurons. **A.** Representative current recordings obtained from one of 7 mouse nodose neurons under control condition (Ctrl), in the presence of 10 µM retigabine (RTG) and after subsequent addition of 10 µM XE991 in the presence of retigabine (RTG+XE). I_M, as defined by XE991-sensitive currents, in the absence (Ctrl) and presence of retigabine (RTG) was derived from the original recordings shown on the upper panel by digital subtraction of the current recorded in the presence of XE991 from that obtained under control condition, and by digital subtraction of the current recorded in the presence of both retigabine and XE991 from that recorded in the presence of retigabine alone, respectively. Dotted line represents the zero-current level. Where the instantaneous (I_{in}) and sustained (I_{SS}) tail currents were measured are indicated. **B**. Mean activation curves obtained from XE991-sensitive tail currents recorded in the absence and presence of 10 µM retigabine (n=6). * p=0.015 at -75 mV, 0.024 at -65 mV, 0.037 at -55 mV, 0.031 at -45 mV and 0.031 at -35 mV by paired t-test or Wilcoxon signed rank test when normality test failed.

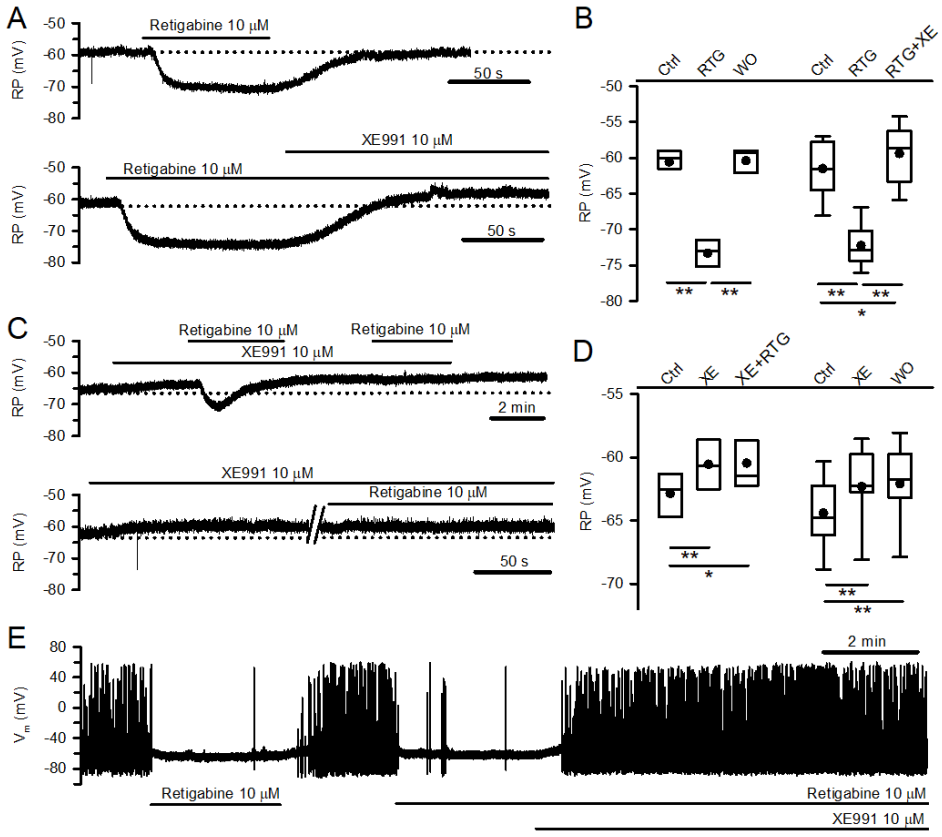

Figure 4. Effects of retigabine and/or XE991 on resting potentials (RP) and spontaneous AP firing in mouse nodose neurons. **A.** Representative recordings of membrane potential obtained from two different neurons. Bath application of retigabine and XE991 are indicated by the horizontal bars on the top of the recordings. Dotted lines indicate the control RP levels. **B.** Quantification of RP values measured from two groups of neurons (n=6 and 12, respectively) under control condition (Ctrl), in the presence of retigabine (RTG) and after washout of retigabine (WO), or after subsequent addition of XE991 to retigabine-containing bath solution (RTG+XE) as the examples shown in panel A. * p=0.006, ** p<0.001. **C.** Representative recordings of membrane potential obtained from two different neurons. Dotted lines indicate the control RP levels. The break sign on the lower trace represents a 5-min interval, during which the cell was repetitively stimulated to fire the APs with suprathreshold current injections in the constant presence of XE991. **D.** Quantification of RP values measured from two groups of neurons (n=8 and 10, respectively) at baseline (Ctrl), in the presence of XE991 (XE) and after addition of retigabine in the presence of XE991 (XE+RTG), or after washout of XE991 (WO). * p=0.004, ** p<0.001. **E.** Representative recordings of membrane potential showing the effects of retigabine and XE991 on spontaneous AP firing. Graphs in B and D show box and whisker plots. The horizontal lines of boxes represent the 25th percentile, the median and the 75th percentile. The whiskers represent the 5th/95th percentile. The filled circles represent the mean values. Statistical significance was determined by one way repeated measures ANOVA with Holm-Sidak test as a *post hoc* analysis.

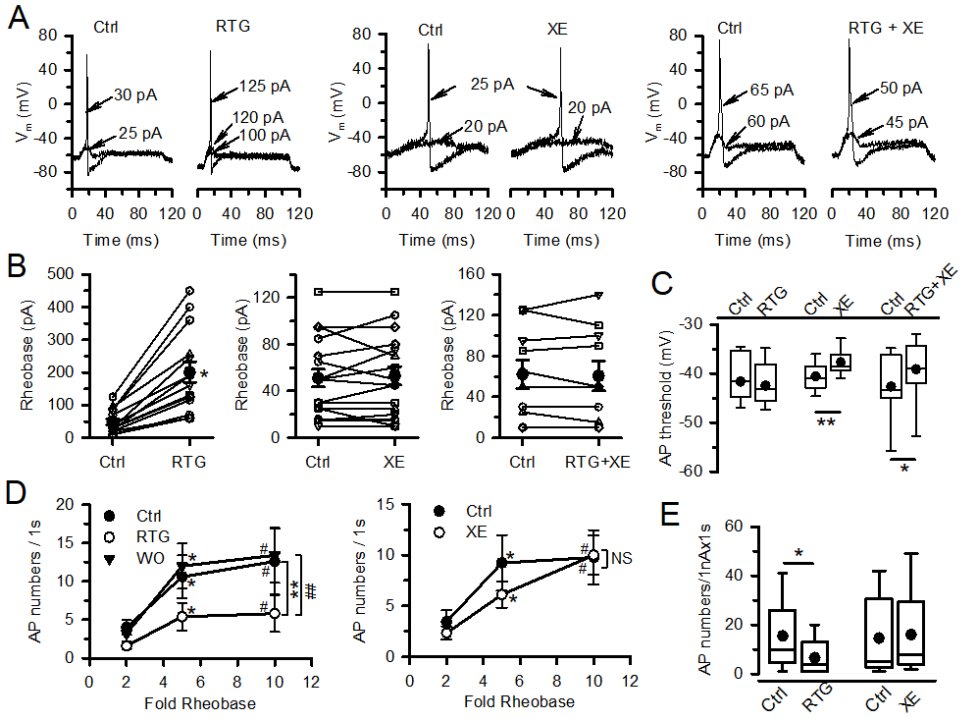

Figure 5. Effects of retigabine and/or XE991 on excitability of mouse nodose neurons. **A.** Representative recordings of membrane potential showing the smallest amount of depolarizing current needed to evoke an AP (rheobase) at baseline (Ctrl) and after application of retigabine (RTG), XE991 (XE) or retigabine in the presence of XE991 (RTG+XE). **B.** Changes in rheobase by retigabine (left, n=14), XE991 (middle, n=18) or retigabine in the presence of XE991 (right, n=10). Open symbols and lines indicate the change for individual cells. Filled circles and error bars represent mean±SEM of the group. * p<0.001 (paired *t*-test). **C.** Quantification of AP threshold obtained from three groups of neurons before (Ctrl) and after application of retigabine (RTG, n=14), XE991 (XE, n=18) or both retigabine and XE991 (RTG+XE, n=10). * p=0.001. ** p<0.001 (paired *t*-test). **D.** *left*: Averaged number of APs evoked by 1-s depolarizing current as a function of the injected current intensity (defined as fold rheobase) obtained from 5 cells in the absence and presence of 10 µM retigabine, and after washout of the drug (WO). * p=0.023, and # p=0.01 compared to AP numbers at 2-fold rheobase. **p=0.008, ## p=0.005 between two conditions as indicated. *Right:* Similar plots of data obtained from 9 cells under control condition and in the presence of 10 µM XE991. * p=0.002, # p<0.001 compared to AP numbers at 2-fold rheobase. NS: P=0.4 between two groups. Statistical significance was determined by two way repeated measures ANOVA with Holm-Sidak test as a *post hoc* analysis. **E.** Quantification of AP numbers in response to the same suprathreshold stimulation (1 nA for 1 s) obtained from 2 groups of neurons before and after treatment with retigabine, and before and after treated with XE991, respectively. n=9 for both groups. * p=0.01 (paired *t*-test). Graphs in **C** and **E** show box and whisker plots. The horizontal lines of boxes represent the 25th percentile, the median and the 75th percentile. The whiskers represent the 5th/95th percentile. The filled circles represent the mean values.

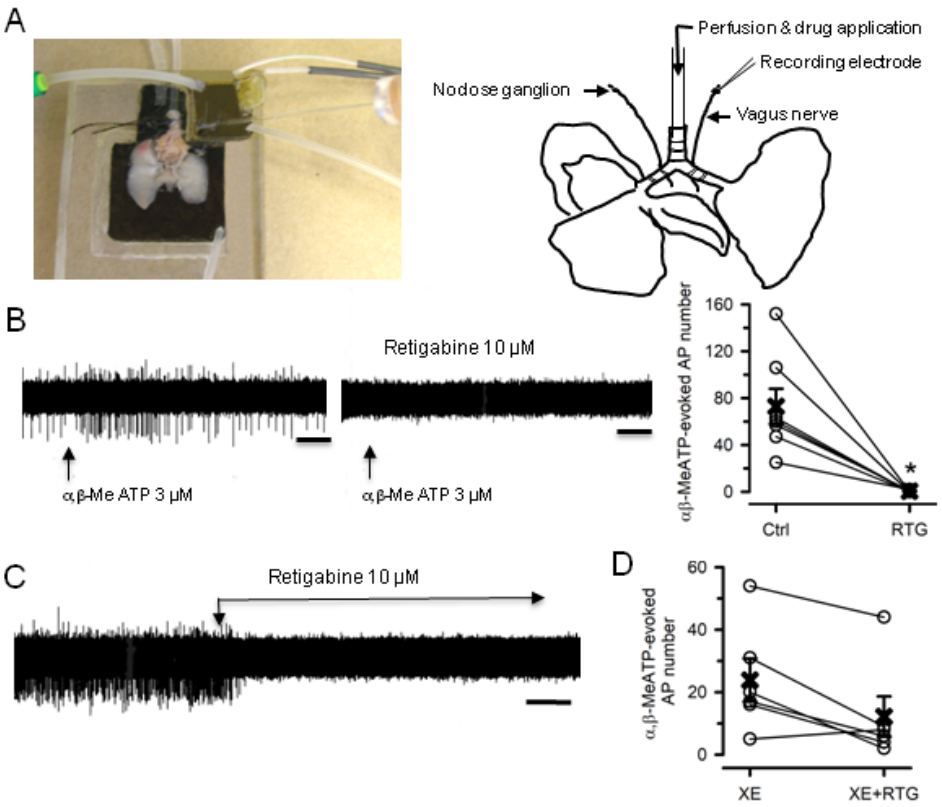

Figure 6. Effects of M-channel modulators on AP discharge in mouse bronchopulmonary nodose C-fibers. **A.** Image (*left*) and schematic representation (*right*) of a trachea-perfused mouse lung-vagus nerve preparation. **B.** Representative traces (*left*) and group data (*right*, n=7) of α,β-MeATP-induced AP firing recorded from mouse lung nodose C-fibers before (Ctrl) and after treatment with retigabine (RTG, 10 µM for 15 mins). The fiber shown on the left responded to α,β-Me ATP with a peak firing frequency of 4 Hz. Calibration bar: 10 s. On the right panel, open symbols and lines indicate the change in AP number for individual fibers. Bold cross and error bars represent mean±SEM of the group * p=0.004 (paired t-test). **C.** Recording from one of four C-fibers exhibiting spontaneous AP firing (<1 Hz) that was silenced by application of retigabine. Calibration bar: 2 mins. **D.** AP numbers in response to 3 µM α,β-MeATP obtained from 6 fibers in the presence of XE991 (XE, 30 µM) and XE991 (30 µM) plus retigabine (10 µM) for 15 mins. The preparations were perfused with normal Krebs solution for 30 mins between treatments. Open symbols and lines indicate the changes for individual fibers. Bold cross and error bars represent mean±SEM. Note AP number in XE991 is less than control (48±24 APs for this group of fibers) which may be due to the inhibition of I_{Na} as discussed. P>0.05 by one-way repeated measures ANOVA.

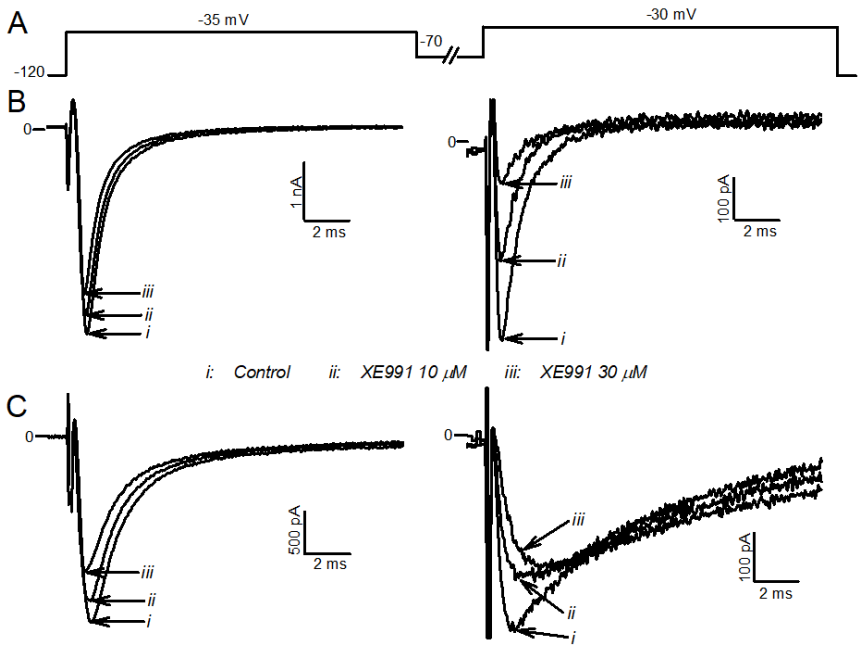

Figure 7. Effects of XE991 on Na^+ currents in mouse nodose neurons. **A.** Voltage-clamp protocol consisting of two depolarizing pulses to voltages at which the I_{Na} peaks, separated by an 1-sec interval at -70 mV (V_h: -120 mV). **B** and **C**. Current recordings elicited by the first (left panels) and the second (right panels) depolarizing step from two different nodose neurons under control condition and after bath application of 10 and 30 µM XE991. Please note the different scales of the *y*-axis among 4 panels. Similar effects were observed in 4 neurons.

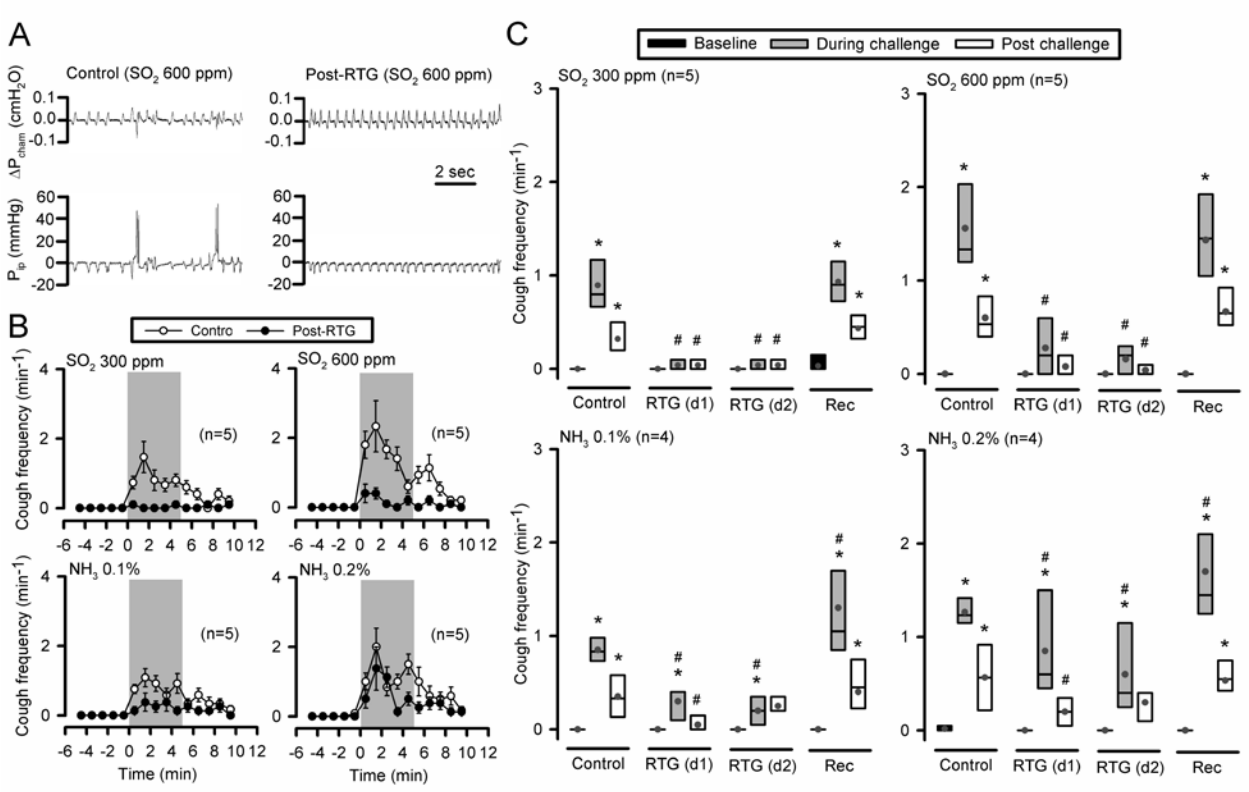

Figure 8. Effects of retigabine on irritant gases-induced coughing in awake mice. **A**. Representative recordings illustrating the effect of nebulized retigabine (RTG) on the cough response to SO_2 inhalation challenge. Note the synchronized changes in both recording chamber pressure (P_{cham}) and intra-pleural pressure (P_{ip}) **B.** Cough frequency in responses to SO_2 or NH_3 inhalation challenges (marked by shaded area) under control conditions and post-RTG treatment. **C.** Box plots of cough frequency at baseline, during and post SO_2 or NH_3 challenge (each from a 5-min recording) before (Control), after RTG inhalation (tested 2 times on 2 different days: d1 & d2) and at least 1 day after the last retigabine inhalation (Rec: recovery). The horizontal lines of boxes represent the 25th percentile, the median and the 75th percentile. The filled circles represent the mean values. * $P < 0.05$ *vs.* baseline; # $P < 0.05$ *vs.* Control (two-way repeated-measures ANOVA with Fisher's test as a *post hoc* analysis for multiple pairwise comparisons). Control data in **B** and **C** were averaged from three experiments performed on three separate days for each mouse, and Post-RTG data in **B** were averaged from two experiments on two separate days for each mouse.

Table 1 : Single cell RT-PCR primer sequences

Gene	Primer	Sequence	Product length
Kcnq2	Forward (5'-3')	TGGTGCTGATTGCCTCCATT	742 bp
	Reverse (3'-5')	CACGGTCTGCCTTTACTTGGT	
Kcnq3	Forward (5'-3')	AGC ACC GTC AGA AGC ACT TT	196 bp
	Reverse (3'-5')	AAG AGA CCC AGC TTT TGG CT	
Kcnq4	Forward (5'-3')	GAG AGC TGG CCC TCT TGT TT	194 bp
	Reverse (3'-5')	GCG GAT TCG GTC TTT GAT GC	
Kcnq5	Forward (5'-3')	GCT CTC GAG GCA GTC AAG ATT	171 bp
	Reverse (3'-5')	ACC GTG ACC TTC CAG TCC TT	
P2rx2	Forward (5'-3')	GGG GCA GTG TAG TCA GCA TC	241 bp
	Reverse (3'-5')	TCA GAA GTC CCA TCC TCC A	
Trpv1	Forward (5'-3')	TCA CCG TCA GCT CTG TTG TC	285 bp
	Reverse (3'-5')	GGG TCT TTG AAC TCG CTG TC	